A Robustness Approach for Handling Modeling Errors in Parallel-Plate Electrostatic MEMS Control

Guchuan Zhu, *Member, IEEE*, Lahcen Saydy, Mehran Hosseini, Jean-François Chianetta, and Yves-Alain Peter, *Senior Member, IEEE*

***Abstract*—This paper addresses the control of electrostatic parallel-plate microactuators in the presence of such modeling errors as unmodeled fringing field effect and deformations. In general, accurate descriptions of these phenomena often lead to very complicated mathematical models, while ignoring them may result in significant performance degradation. In this paper, it is shown by finite-element-method-based simulations that the capacitance due to fringing field effect and deformations can be compensated by introducing a variable serial capacitor. When a suitable robust controller is used, the full knowledge of the introduced serial capacitor is not required, but merely its boundaries of variation. Based on this model, a robust control scheme is derived using the theory of input-to-state stability combined with backstepping state feedback design. Since the full state measurement may not be available under practical operational conditions, an output feedback control scheme is developed. The stability and performance of the system using the proposed control schemes are demonstrated through both stability analysis and numerical simulation. The present approach allows the loosening of the stringent requirements on modeling accuracy without compromising the performance of control systems. [2007-0262]**

***Index Terms*—Control systems, electrostatic actuators, microelectromechanical devices, nonlinear systems, robustness, uncertainty.**

NOMENCLATURE

A	Cross-sectional area of each of the electrodes.
b	Damping coefficient.
C_0	Zero-voltage capacitance.
C_a	Capacitance of the actuator.
C_p	Parallel capacitance.
C_s	Serial capacitance.
G	Air gap.
G_0	Zero-voltage gap.
I_s	Source current.
I_a	Current through the actuator.
I_p	Current through the parallel capacitor.
k	Stiffness coefficient.
m	Mass of the moveable electrode.
Q_a	Charge on the actuator.
Q_p	Charge on the parallel capacitor.
R	Loop resistance.
V_a	Voltage across the actuator.
V_p	Voltage across the parallel capacitor.
V_s	Source voltage.
ϵ	Permittivity constant.
ρ_p	Parallel capacitive influence coefficient.
ρ_s	Serial capacitive influence coefficient.
ω_0	Undamped natural frequency.

Manuscript received October 31, 2007; revised July 1, 2008. First published October 28, 2008; current version published December 4, 2008. This work was supported in part by the Natural Sciences and Engineering Research Council of Canada. Subject Editor N. Aluru.

G. Zhu and L. Saydy are with the Electrical Engineering Department, École Polytechnique de Montréal, Montréal, QC H3C 3A7, Canada (e-mail: guchuan.zhu@polymtl.ca).

M. Hosseini and Y.-A. Peter are with the Engineering Physics Department, École Polytechnique de Montréal, Montréal, QC H3C 3A7, Canada.

J.-F. Chianetta is with Coventor SARL, 91140 Villebon sur Yvette, France.

Color versions of one or more of the figures in this paper are available online at http://ieeexplore.ieee.org.

Digital Object Identifier 10.1109/JMEMS.2008.2005291

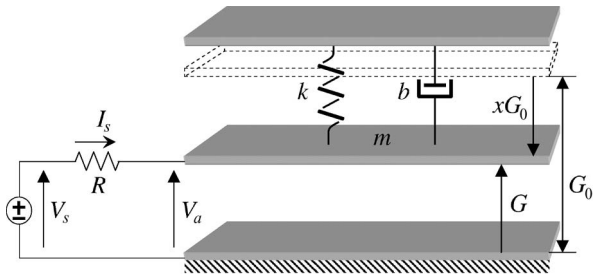

Fig. 1. Schematic representation of 1DOF parallel-plate electrostatic actuator. The top structure is fixed for sustaining the moveable plate.

I. INTRODUCTION

THIS PAPER addresses the control of electrostatic parallel-plate actuators, whose schematic representation is shown in Fig. 1 where m is the mass of the moveable plate, k is the stiffness coefficient, b is the damping coefficient, G is the air gap, G_0 is the zero-voltage gap, x is the normalized displacement, R is the loop resistance, V_a is the voltage across the actuator, and V_s and I_s are the source voltage and current, respectively. For simplicity, only the representative model components are presented. As the electrostatic force is always attractive regardless of the sign of the driving source, the device can be grounded by either the moveable plate or the fixed electrode for the convenience of the design or considerations of applications. Therefore, the ground is not shown. The actuator is supposed to make only one degree-of-freedom (1DOF) piston motion.

In the most popular model of such devices, the moveable plate is supposed to be a rigid body without deformation, and only the main electric field within the gap is considered, without fringing fields. That is, since the gap is relatively small, the

capacitance can be approximated as being a small portion of an infinite parallel plate (see, e.g., [1]). The actuator capacitance can then be computed by

$$C_a = \frac{\epsilon A}{G} \tag{1}$$

where A is the area of the side of an electrode plate facing the gap and ϵ is the permittivity in the gap. Equation (1) is of course a simplified model, which is subject to modeling errors due to, e.g., deformations, fringing field effect, and parasitics. Fabrication deviations and environmental fluctuations may also introduce parameter variations affecting the reliability of the model. Therefore, the performance of control schemes based on this simplified model may be compromised for applications in which precise positioning is required, e.g., adaptive optics (see, e.g., [2]). Later on, in Section II-A, we present an analysis of the influence of certain modeling errors on the static behavior of the actuator.

To obtain high performance, one may need to use a more accurate model. There is a continuous effort in the literature to improve the modeling accuracy of electrostatic devices and MEMS by taking into account practical considerations, such as the effect of fringing fields [3]–[9], deformation [10], [11], and surface charge density singularities at sharp corners and edges [12]. One can find a rich set of research results on the modeling of MEMS in the literature (see, e.g., [13] and [14]). In general, accurate modeling results, however, in a more complex mathematical model which makes control systems more complicated and harder to implement, although it undoubtedly helps increase the performance of software tools for MEMS simulation and design. More specifically, modeling fringing fields and deformations lead, in general, to distributed parameter systems described by partial differential equations (see, e.g., [9] and [11]). The control of such systems requires distributed sensing and actuation, and hence, it is very hard to implement for microsystems (see, e.g., [15]). Other sources of uncertainty, such as parasitics, complicate the modeling issue even further. In addition, most of the existing formulations do not precisely represent the behavior of real devices due to dielectrics, imperfect conductors, rough sidewalls, rounded corners, etc. In [16], a generic capacitive model of electrostatic parallel-plate actuators has been proposed. This model is based on the simplified one given in (1) while presenting diverse unmodeled phenomena by serial and parallel capacitors. The equation of motion of such a model can be expressed by ordinary differential equations. However, it is difficult to determine the values of the serial and parallel capacitors which depend on the aforementioned physical phenomena.

The present work is motivated by that of [16], and the objective is one of modeling the plant for the purpose of controlling it. As such, the model sought needs to capture the essential dynamical behavior of the system and yet be simple enough to make the control design less complicated in terms of implementability as well as closed-loop performance. It has been shown in [17] that the effect of fringing fields can be modeled by a variable serial capacitor. In this work, we extend this method to a deformed structure and show that, in the presence of deformation, the modeling error can also be compensated by introducing a suitable serial capacitor. The advantage of this approach is that, combined with an appropriate robust control scheme, the full knowledge of the introduced serial capacitor is not required, but merely that of its boundaries of variation. These can be estimated by finite-element-method (FEM)-based simulations using commercial off-the-shelf software tools, e.g., ANSYS, COMSOL, and CoventorWare, or obtained by experimental measurements. This idea can considerably simplify the modeling toward control of such complex systems without compromising the closed-loop performance.

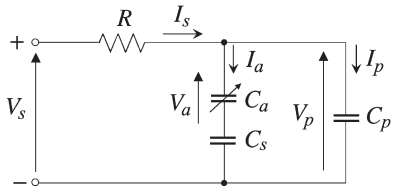

Fig. 2. Equivalent circuit of 1DOF parallel-plate electrostatic actuator with parallel and serial capacitors.

The robust control schemes used in this work are based on the theory of input-to-state stability (ISS) [18], [19] and backstepping design [20]. The nominal model used in control law design is the simplified parallel-plate actuator whose capacitance is given in (1), but the controller is made robust against certain modeling errors. Note that the ISS-based control design can also incorporate parameter uncertainties due to, e.g., variation of damping ratio and loop resistance, as done in [21] as well as here. The stability and the performance of the system using these control schemes are tackled through both stability analysis and numerical simulation.

The remainder of this paper is organized as follows. Section II presents the model of a general 1DOF parallel-plate electrostatic actuator. Sections III and IV are devoted to state feedback and output feedback control designs, respectively. The simulation results are reported in Section V, and Section VI contains some concluding remarks.

II. Dynamics of a Generic Capacitive Model of Parallel-Plate Electrostatic Microactuator

A. Dynamics of a Generic Capacitive Model

The equation of motion of 1DOF parallel-plate microactuators driven by an electrostatic force is given by (see, e.g., [1])

$$m\ddot{G} + b\dot{G} + k(G - G_0) = F_e \tag{2}$$

where the electrostatic force F_e is given by

$$F_e = \frac{V_a^2}{2}\frac{\partial C_a}{\partial G} = -\frac{2\epsilon A V_a^2}{G^2} = -\frac{Q_a^2}{2\epsilon A} \tag{3}$$

and V_a is the voltage across the actuator, and Q_a is the charge on the actuator.

Fig. 2 shows the equivalent circuit of a 1DOF parallel-plate electrostatic actuator containing serial and parallel capacitors, denoted by C_s and C_p, respectively. In Fig. 2, we also show the currents through the actuator (and the serial capacitor) and

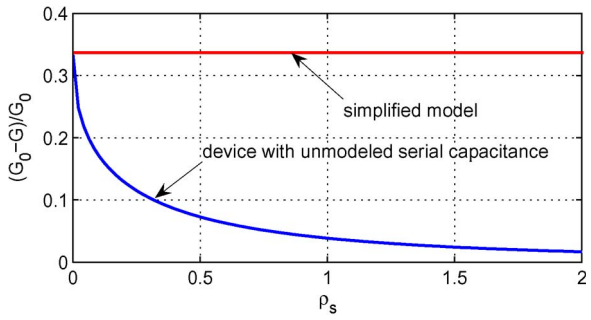

Fig. 3. Influence of serial capacitive uncertainty to static behavior of parallel-plate devices.

the parallel capacitor I_a and I_p, respectively, and the voltage across the parallel capacitor V_p. We suppose that there is no current leakage across the device. In our model, the serial and parallel capacitors are expressed in terms of what we refer to as *capacitive influence coefficients*, defined as

$$\rho_s \triangleq \frac{C_0}{C_s} \qquad \rho_p \triangleq \frac{C_p}{C_0} \tag{4}$$

where C_0 is the capacitance of the actuator at the zero-voltage position. Note that, in the present work, C_0 is a known quantity, and C_s and C_p represent modeling errors, but not actual physical elements in the structure. The dynamical equation of the electrical subsystem is then given by [21][1]

$$\dot{Q}_a = \frac{1}{R\left(1+\rho_p\rho_s+\rho_p\frac{G}{G_0}\right)} \times \left(V_s - \left(\frac{G}{\epsilon A}+\rho_s\frac{G_0}{\epsilon A}+R\rho_p\frac{\dot{G}}{G_0}\right)Q_a\right) \tag{5}$$

in which the source voltage V_s is the actual control variable. Note that, following the same line of reasoning, we can model the devices with more complicated configurations including, e.g., current leak.

The model described previously captures a quite wide range of modeling errors. For example, the serial capacitor can characterize, as we will see later, the effect of fringing fields and deformations, and the parallel capacitor can represent the parasitics. Clearly, the higher the values of ρ_s and ρ_p, the more important the influence of the modeling errors. When the capacitive influence coefficients are set to zero, the dynamics of the electrical subsystem boil down to

$$\dot{Q}_a = \frac{1}{R}\left(V_s - \frac{Q_a G}{\epsilon A}\right) \tag{6}$$

which is the most popular one used in the literature (see, e.g., [1]). Note that, since the nominal plant is an ideal rigid body, the dynamics of the mechanical subsystem still follow (2). Therefore, with the presented model, the serial and parallel capacitors affect only the dynamics of the electrical subsystem.

[1]For readers' convenience, the development of (5) is given in Appendix I.

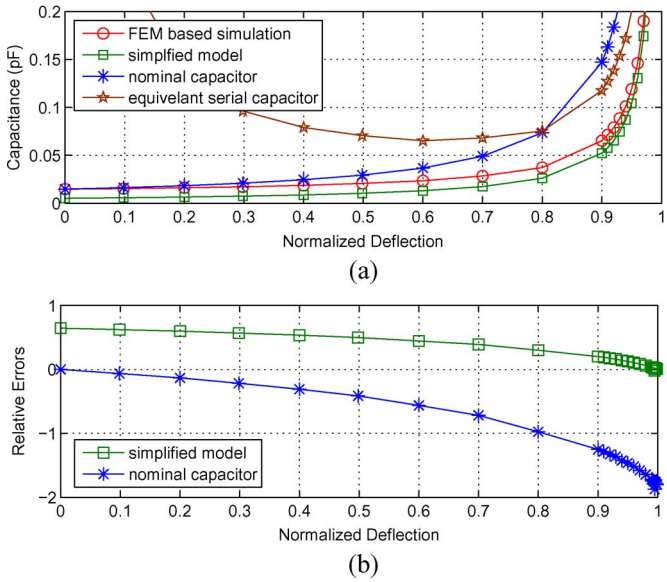

Fig. 4. Capacitances of the structure in the presence of fringing fields: (a) FEM-based simulation, simplified model, nominal capacitor, and equivalent serial capacitor. (b) FEM relative error simulation.

It can be seen from (5) that the parallel capacitor will not change the static behavior of the device. It does, however, affect the dynamics of the electrical subsystem: The bigger the parallel capacitance, the slower the dynamics of the driving circuit. The serial capacitor will affect both the static and dynamic behaviors of the system. In particular, it will change the pull-in position. To see this, we consider an example from [21], shown in Fig. 3. The static positions (equilibrium points) of the device can be deduced from (2) and (5) by setting all derivatives to zero

$$0 = k(G-G_0)+\frac{Q_a^2}{2\epsilon A}$$
$$0 = V_s - \left(\frac{G}{\epsilon A}+\rho_s\frac{G_0}{\epsilon A}\right)Q_a.$$

In this example, the input V_s is set to the pull-in voltage $\sqrt{8kG_0^3/27\epsilon A}$ [1]. In the simplified model, $\rho_s = 0$. Therefore, the normalized static position, defined by $(G_0 - G)/G_0$, is 1/3. However, it can be seen that the static position varies with respect to serial capacitive uncertainty, represented by ρ_s, and does so in an abrupt manner precisely for unmodeled serial capacitance due to, e.g., ignored fringing fields. In open-loop control schemes, this may result in significant regulation errors if the simplified model is used to predict the deflections of the device.

B. Effect of Fringing Fields

In order to examine the effect of fringing fields, we simulated a parallel-plate actuator with rectangular electrodes of width $W = 600$ μm, length $L = 300$ μm, and initial separation distance $G_0 = 305$ μm. The gap of the considered structure is intentionally made big so that the fringing fields are not negligible. Fig. 4 shows the simulated capacitance of the device obtained using CoventorWare, presented as a function of the normalized deflection from the zero-voltage position. Note that,

in the simulation, a mechanical distributed force (pressure), rather than an actuation voltage, has been applied to the structure to produce deflections and, eventually, deformations. This allows the computation of the capacitance of the structure over the whole gap range without suffering from the pull-in. As can be seen from Fig. 4, at the initial stage when the gap is comparable to the full extent of the electrodes, the simplified model considerably underestimates the value of the capacitance (about 35% of the simulated structure). Decreasing the gap will attenuate the effect of fringing fields, and when both W/G and L/G become more than 100, the difference becomes less than 5%.

Clearly, the fringing fields have the effect of increasing the capacitance and the charge on the device. Hence, it will increase the electrostatic force as well. However, the influence of fringing fields decreases as the gap closes. Therefore, we can use an overestimated nominal capacitor, denoted by C_n, combined with an appropriate variable serial capacitor to represent the total capacitance of the device. At the zero-voltage position, C_n has the same value as that of the device accounting for fringing fields, but its variation versus deflections follows (1) instead. Obviously, to satisfy these conditions, the effective electrode areas of C_n must be larger than that of the actual structure. The value of the introduced serial capacitor is a function of the gap and can be expressed as

$$\frac{1}{C_s} = \frac{1}{C_a} - \frac{1}{C_n}. \tag{7}$$

Fig. 4 shows the capacitances of the simplified model computed by (1), the simulated device, the nominal capacitor, and the introduced serial capacitance computed from (7). The value of the nominal capacitor at the zero-voltage position is equal to 1.47×10^{-2} pF (the same as the capacitance of the simulated structure at the same position). We can see that, except for the initial separation distance, there is a difference between the value of the nominal capacitor and the one of the simulated structure. The role of the serial capacitor is to compensate for this deficit. As shown in Fig. 4, the value of the serial capacitance is infinite at the zero-voltage position and has a minimum that is about 6.47×10^{-2} pF for this structure. Since the smaller the introduced serial capacitance, the bigger the influence of modeling errors, we can use its minimum value to determine the upper bound of the serial capacitive influence coefficient $\overline{\rho}_s$. For example, for the structure shown in Fig. 4, $\overline{\rho}_s = 1.47/6.47 = 0.2272$.

In practice, since C_a is not exactly known if the fringing fields are not modeled, one cannot determine C_s for every deflection. However, as mentioned earlier and as will be seen later, for an appropriate robust control scheme, only the upper bound of the serial capacitive influence coefficient, corresponding to the minimum of C_s, is required in the design of control laws. This would allow one to drastically reduce the modeling complexity. Note that the numerical simulation might significantly deviate from the real device. In this case, a conservative boundary should be used in control design. This may result in a higher control effort. Nevertheless, the performance is guaranteed as long as the actual modeling errors do not exceed the boundaries.

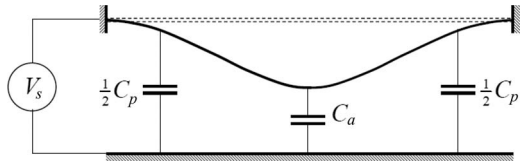

Fig. 5. Schematic representation of deformed structures.

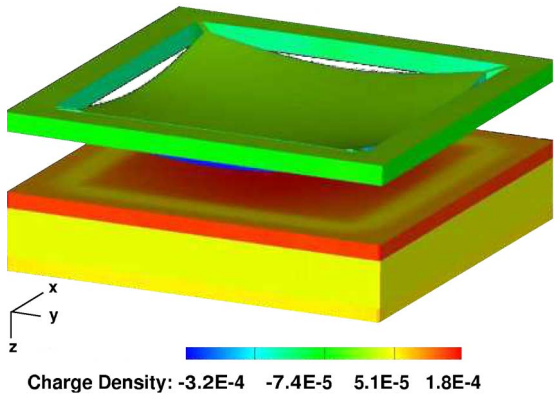

Fig. 6. FEM-based simulation of a deformed microstructure.

C. Deformed Devices

When deformations happen, the displacement is no longer uniform: the deformation in the center portion is largest, whereas the portions near the step-up supports hardly move at all. Conceptually, the overall capacitance of a deformed device can be represented by the sum of two 1-D capacitors: a variable capacitor, representing the effective actuator, in parallel with another one whose equivalent surface is parameterized by the air gap (Fig. 5). The total capacitance of such devices can be expressed as [16]

$$C_{\text{total}} = C_a + C_p \propto \frac{1-\gamma}{G} + \frac{\gamma}{G_0} \tag{8}$$

where C_a is the capacitance that contributes to electrostatic force, C_p is the capacitance corresponding to the portion that does not generate electrostatic force, and γ is a proper function that increases as the gap closes. Obviously, it is very difficult to determine the function γ in (8), because it changes with the boundary condition, the geometry, and the mechanical structure of the actuator.

To examine the effect of deformation, we have simulated another microstructure using CoventorWare. The electrode dimensions are 206×206 μm^2, and the moveable plate is sustained by four beams clamped at the corners. The thickness of the moveable plate is 1.5 μm, and the initial gap is 5 μm. Note that, as the air gap of this device is much smaller than its geometrical extent, the effect of fringing fields will not be significant. The deformation and the distribution of charge density at an intermediate position is shown in Fig. 6. The technique mentioned in Section II-B is used to simulate the capacitance over the whole gap range, and the results are shown in Fig. 7. It can be seen that, for small deflections, the capacitance of the simulated device is higher than the one calculated from the rigid body approximation given by (1) (about 17% higher at the

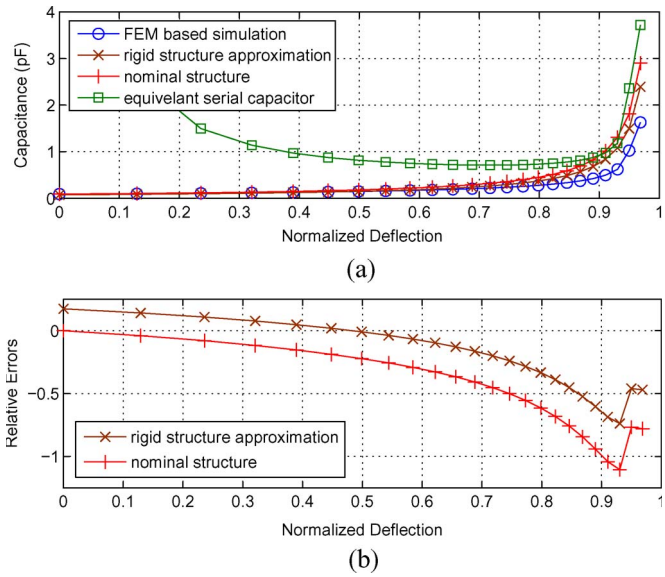

Fig. 7. Capacitances of deformed structure. (a) Capacitances of FEM-based simulation, rigid structure approximation, nominal structure, and equivalent serial capacitor. (b) Relative errors to FEM-based simulation.

zero-voltage position). This is due to unmodeled phenomena, e.g., the electrostatic force due to the capacitance between the flexures and the substrate. For large deflections, the deformation becomes important. In this case, the capacitance computed from (1) is overestimated. For a deflection of 4.8431 μm, the modeling error can be as high as 47%. Since the effect of fringing fields decreases as the gap closes, the modeling error for large deflections is mainly due to the deformation.

The modeling error due to deformation can be compensated by an appropriate variable serial capacitor as well. More precisely, we first model the device as an ideal rigid body, also called the nominal structure. If we take also into account the effect of fringing fields, the capacitance of the nominal structure C_n follows the simplified model given in (1), but uses an effective area A_{eff} to match the actual value of the capacitance at the zero-voltage position. Since the deformation has the effect of decreasing the capacitance and the effect of fringing fields is maximum at the zero-voltage position, the nominal structure gives overestimated capacitance for any nonzero deflection. The introduced serial capacitor has the effect of reducing the total capacitance, and hence, it will eliminate the modeling error.

The capacitances of the nominal structure and the introduced serial capacitor are also shown in Fig. 7. The latter one is computed from (7) using the capacitances of the simulated device and the nominal structure. The value of the nominal capacitor at the zero-voltage position is equal to 0.0909 pF (the same as the simulated capacitor at this position). As shown in Fig. 7, the introduced serial capacitance is infinite at the zero-voltage position and has a minimum of about 0.7126 pF, which can be used to determine the upper bound of the serial capacitive influence coefficient $\overline{\rho}_s$. For this structure, we have $\overline{\rho}_s = 0.0909/0.7126 = 0.1277$.

It is worth noting that, theoretically, the surface charge density is infinite at sharp corners and edges (see [12] and the references therein). The accuracy of the simulation methods could be affected by these geometrically induced singularities. In general, the omission of charge distribution singularity results in an underestimated electrostatic force. This modeling error can also be compensated by using a more conservative bound in our model.

Finally, the parallel parasitics is a relatively well-understood phenomenon. The unmodeled parallel capacitance can be determined by numerical simulation or experimental measurements. We will see later on that the proposed robust control laws work well with very conservative estimates of parallel capacitive influence coefficient. Therefore, the presence of this type of modeling errors will not introduce technical difficulties for applying these control laws.

III. Robust Control by State Feedback

A. Preliminaries on ISS

The concept of ISS was introduced by [18], and ISS-based design is a popular tool in the field of nonlinear control. Here, we only present the notations required in the development of the control law. The interested reader is referred to, for example, [19] and [20] for a formal presentation.

The following comparison functions are required for presenting the method of ISS. A function $\alpha : [0, a) \to [0, \infty)$ is said to belong to Class $\mathcal{K}$ if it is continuous, strictly increasing, and $\alpha(0) = 0$. If $a = \infty$ and α is unbounded, the function is said to belong to Class $\mathcal{K}_\infty$. A function $\beta : [0, a) \times [0, \infty) \to [0, \infty)$ is said to belong to Class $\mathcal{KL}$ if it is nondecreasing in its first argument, nonincreasing in its second argument, and $\lim_{s\to 0^+} \beta(s, t) = \lim_{t\to\infty} \beta(s, t) = 0$.

The system

$$\dot{x} = f(x, u) \tag{9}$$

is said to be input-to-state stable (also denoted by ISS for convenience) if, for any $x(0)$ and for any bounded continuous input $u(\cdot)$ on $[0, \infty)$, the solution exists for all $t \geq 0$ and satisfies

$$|x(t)| \leq \beta(\|x(0)\|, t) + \gamma\left(\sup_{0\leq\tau\leq t} \|u(\tau)\|\right) \qquad \forall t \geq 0 \tag{10}$$

for some $\beta \in \mathcal{KL}$ and $\gamma \in \mathcal{K}$.

System (9) is ISS if and only if there exists a smooth positive definite radially unbounded function V and class $\mathcal{K}_\infty$ functions α_1 and α_2 such that the time derivative of V along the solutions of (9) verifies

$$\dot{V} = \frac{\partial V}{\partial x} f(x, u) \leq -\alpha_1(\|x\|) + \alpha_2(\|u\|). \tag{11}$$

The function V satisfying the aforementioned inequality is called an ISS control Lyapunov function (CLF).

One advantage of the ISS approach is that it provides a convenient framework for robust system control, which amounts to finding a control for which the closed-loop system is stable with respect to disturbances, considered now as inputs to the system.

B. State-Space Model in Normalized Coordinates

To make the system analysis and control design easier, we transform (2) and (5) into normalized coordinates by changing the time scale $\tau = \omega_0 t$ and performing a normalization as follows [22], [23]:

$$x = 1 - \frac{G}{G_0} \qquad q = \frac{Q_a}{Q_{\rm pi}}$$
$$u = \frac{V_s}{V_{\rm pi}} \qquad i = \frac{I_s}{V_{\rm pi}\omega_0 C_0}$$
$$r = \omega_0 C_0 R$$

where $V_{\rm pi} = \sqrt{8kG_0^2/27C_0}$ is the nominal pull-in voltage, $Q_{\rm pi} = (3/2)C_0 V_{\rm pi}$ is the nominal pull-in charge, and $\omega_0 = \sqrt{k/m}$ is the undamped natural frequency. We then have

$$\frac{d^2x}{d\tau^2} + 2\zeta\frac{dx}{d\tau} + x = \frac{1}{3}q^2 \tag{12a}$$

$$\frac{dq}{d\tau} = \beta\left(\frac{2}{3}u - (1-x)q - \rho_s q + r\rho_p q\frac{dx}{d\tau}\right) \tag{12b}$$

where $\zeta = b/2m\omega_0$ is the damping ratio and

$$\beta = \frac{1}{r\left(1 + \rho_p(1-x) + \rho_p\rho_s\right)} \tag{13}$$

is a function of the deflection.

Letting $x_1 = x$, $x_2 = dx/d\tau$, and $x_3 = q^2$, the aforementioned system can then be written in normalized state-space coordinates as

$$\frac{dx_1}{d\tau} = x_2 \tag{14a}$$

$$\frac{dx_2}{d\tau} = -2\zeta x_2 - x_1 + \frac{1}{3}x_3 \tag{14b}$$

$$\frac{dx_3}{d\tau} = \beta\left(\frac{4\sqrt{x_3}}{3}u - 2(1-x_1)x_3 - 2\rho_s x_3 + 2r\rho_p x_2 x_3\right). \tag{14c}$$

System (14) is defined on the state space $\mathcal{X} = \{(x_1, x_2, x_3) \in \mathbb{R}^3 | x_1 \le 1, x_3 \ge 0\}$.

Note that the considered actuator exhibits switching behavior. First of all, when the moveable plate hits the fixed one $(x_1 = 1)$, the dynamics of the mechanical subsystem collapse [24]. In addition, $q = 0$ $(x_3 = 0)$ is a singular point at which system (14) is not linearly controllable (see, e.g., [24]). However, it is easy to see that the system is symmetric except for the sign of the charge. For simplicity, we ignore the contact dynamics and consider only the branch defined by (14c). Consequently, the stability property obtained through the proposed control will be held locally.

Since in what follows we deal only with normalized quantities, we can use t to denote the time and omit the qualifier "normalized."

C. Control Synthesis

In this work, we also consider parametric uncertainties, such as the variations of the damping and the loop resistance. Note that the damping in microstructures are more accurately modeled as a squeezed film (see, e.g., [25]). In fact, this nonlinear model can be captured in the design of control systems, while the parameter variation can be handled in the same way as the one presented in this work. Similarly, this approach applies to the compensation of the nonlinearity related to the stiffness.

We now make the following assumptions on the uncertainties in system (14).

Assumption 1: The serial and parallel capacitances are bounded by known constants

$$0 \le \rho_p \le \bar{\rho}_p \qquad 0 \le \rho_s \le \bar{\rho}_s. \tag{15}$$

Assumption 2: The damping ratio is positive and bounded and can be written as

$$\zeta = \zeta_0 + \Delta\zeta \tag{16}$$

where ζ_0 is a positive constant representing the nominal damping ratio and $\Delta\zeta$ is the modeling error.

Assumption 3: The upper and lower bounds of the resistance in the loop r are known

$$0 < \underline{r} \le r \le \overline{r}. \tag{17}$$

Since $x_1 \le 1$, β in (13) may be bounded as follows:

$$0 < \underline{\beta} \le \beta \le \overline{\beta} \tag{18}$$

where $\overline{\beta} = 1/\underline{r}$. Note that, since the electrostatic force is always attractive, the control allowing the moveable plate to move as far as possible beyond the initial gap is the one that can remove the charge from the device in an arbitrary small time interval. However, there is no equilibrium beyond the zero-voltage gap, and the mechanical subsystem (14a)–(14b) globally exponentially converges to the origin with zero input $(x_3 = 0)$ (see, e.g., [26]). This implies that x_1 should not be smaller than -1, corresponding to a 100% overshoot when the gap is completely closed. Therefore, in a normal operational condition, β should be lower bounded by

$$\underline{\beta} = \frac{1}{\overline{r}\left(1 + \overline{\rho}_p(2 + \overline{\rho}_s)\right)}. \tag{19}$$

Furthermore, the variation of β is denoted by

$$|\beta - \beta_0| \le \overline{\beta} - \underline{\beta} \triangleq \Delta\beta \tag{20}$$

where β_0 is the nominal value of β.

The design of a robust control law is based on ISS. Some standard tools, such as backstepping [20] and the small-gain theorem [27]–[29], are available for tackling this problem. The control objective is to bring the device to specified set points. The tracking control with $y = x_1$ as the output is considered; therefore, the required performance, such as rise and settling times, can be specified through reference trajectories.

Following a classical approach, we choose a sufficiently smooth reference trajectory y_r for x_1. We then use the approach of backstepping to synthesize a controller that makes the reference trajectory attractive.

The control design consists in constructing an ISS CLF for system (14) via backstepping. The synthesis contains three steps corresponding to three subsystems expressed in (14).

Step 1: Consider the control of the subsystem (14c) with x_2 as a virtual input. Let $z_1 = x_1 - y_r$ be the position tracking error and select a Lyapunov-like function

$$V_1 = \frac{1}{2}z_1^2.$$

The time derivative of V_1 along the solutions of (14c) is

$$\dot{V}_1 = z_1(x_2 - \dot{y}_r).$$

The desired input (also called stabilizing function) can be chosen as

$$x_{2d} = \dot{y}_r - k_1 z_1, \quad k_1 > 0. \tag{21}$$

Step 2: Consider now the subsystem (14a)–(14b) with x_3 as a virtual input. Define $z_2 = x_2 - x_{2d}$ and augment V_1 to yield

$$V_2 = V_1 + \frac{1}{2}z_2^2.$$

Letting $z_3 = x_3 - x_{3d}$, the time derivative of V_2 along the solutions of the corresponding subsystem is given by

$$\begin{aligned}\dot{V}_2 &= -k_1 z_1^2 + z_2\left(z_1 + \dot{x}_2 - \dot{x}_{2d}\right)\\ &= -k_1 z_1^2 + z_2\left(z_1 - 2(\zeta_0+\Delta\zeta)x_2 - x_1 + \frac{1}{3}(z_3+x_{3d}) - \dot{x}_{2d}\right).\end{aligned}$$

In order to counteract the uncertainty $\Delta\zeta$, a nonlinear damping term should be added to the stabilizing function. The desired input in this case is of the following form:

$$x_{3d} = 3\left(2\zeta_0 x_2 + x_1 + \dot{x}_{2d} - z_1 - \kappa_2\zeta_0 x_2^2 z_2 - k_2 z_2\right) \tag{22}$$

where $k_2 > 0$ and κ_2 is the gain of the nonlinear damping term, the lower bound of which will be given later on.

Step 3: Finally, the Lyapunov function candidate for system (14) is chosen to be

$$V_3 = V_2 + \frac{1}{2}z_3^2 = \frac{1}{2}z_1^2 + \frac{1}{2}z_2^2 + \frac{1}{2}z_3^2$$

the time derivative along the solutions of system (14) of which is given by

$$\begin{aligned}\dot{V}_3 = &-k_1 z_1^2 - k_2 z_2^2 - 2\Delta\zeta x_2 z_2 - \kappa_2\zeta_0 x_2^2 z_2^2\\ &+ z_3\left(\frac{z_2}{3} - 3(ab_1+b_2) + 6\Delta\zeta b_1 x_2\right.\\ &\left.+ \beta\left(4\sqrt{\frac{x_3}{3}}u - 2x_3(1-x_1) + 2r\rho_p x_2 x_3 - 2\rho_s x_3\right)\right)\end{aligned} \tag{23}$$

where

$$\begin{aligned}a &= -2\zeta_0 x_2 - x_1 + \frac{1}{3}x_3\\ b_1 &= 2\zeta_0 - k_1 - k_2 - \kappa_2\zeta_0\left(2x_2 z_2 + x_2^2\right)\\ b_2 &= y_r^{(3)} + k_1\ddot{y}_r + \dot{y}_r + \left(\kappa_2\zeta_0 x_2^2 + k_2\right)\dot{x}_{2d}.\end{aligned}$$

Let $U = (4/3)\sqrt{x_3}u$. The proposed backstepping controller is given by

$$\begin{aligned}U = &2x_3(1-x_1) + \frac{3}{\underline{\beta}}\left(ab_1 + b_2 - \frac{z_2}{9}\right) - \frac{1}{\underline{\beta}}k_3 z_3\\ &- \frac{1}{\underline{\beta}}\kappa_{31}\left(ab_1 + b_2 - \frac{z_2}{9}\right)^2 z_3 - \frac{1}{\underline{\beta}}\kappa_{32}\zeta_0 b_1^2 x_2^2 z_3\\ &- \frac{1}{\underline{\beta}}\kappa_{33}x_2^2 x_3^2 z_3 - \frac{1}{\underline{\beta}}\kappa_{34}x_3^2 z_3\end{aligned} \tag{24}$$

with $k_3 > 0$, where κ_{31}, κ_{32}, κ_{33}, and κ_{34} are the gains of the nonlinear damping terms.

Theorem: For system (14) with the uncertainties satisfying Assumptions 1–3 and y_r being sufficiently smooth, the backstepping controller specified by (24), with

$$\kappa_2 > \frac{1}{2\zeta_0} \quad \kappa_{31} > 1 \quad \kappa_{32} > \frac{1}{\zeta_0} \quad \kappa_{33} > 1 \quad \kappa_{34} > \frac{1}{\underline{r}^2} \tag{25}$$

renders the closed-loop error dynamics locally ISS with respect to the uniformly bounded inputs $\Delta\beta$, ρ_p, ρ_s, and $\Delta\zeta$. Furthermore, the ultimate bound for the tracking error z_1 can be rendered arbitrarily small by picking the feedback gains k_1, k_2, and k_3 large enough.

The proof of Theorem 1 is provided in [21].

Note that the actual control u is singular when $x_3 = 0$. This is due to the uncontrollability of system (14) at the zero-voltage position. However, this situation happens only at this point. It is easy to see that system (14) is stable at this position with an input $u = 0$. By defining an open ball $B_\varepsilon = \{X|\ \|X\| < \varepsilon\} \subset \mathcal{X}$ of radius ε centered at the origin, where $X = (x_1, x_2, x_3)^{\mathrm{T}}$ and $\|\cdot\|$ is the usual Euclidean norm, a more practical control law can be expressed as

$$u = \begin{cases} \frac{3}{4\sqrt{x_3}}U, & \text{for } X \notin B_\varepsilon \\ 0, & \text{for } X \in B_\varepsilon \end{cases} \tag{26}$$

where U is given by (24).

D. Reference Trajectory Design

In general, reference trajectories can be chosen to be any sufficiently smooth function $y(t)$ connecting the initial point at time t_i to a desired point at time t_f, such that the initial and final conditions are verified. The reference trajectory used in our control schemes is a polynomial of the following form:

$$y_r(t) = y(t_i) + (y(t_f) - y(t_i))\,\tau^5(t)\sum_{i=0}^{4} a_i\tau^i(t) \tag{27}$$

where $\tau(t) = (t - t_i)/(t_f - t_i)$. For a set-point control, the coefficients in (27) can be determined by imposing the initial and final conditions

$$\dot{y}(t_i) = \dot{y}(t_f) = \ddot{y}(t_i) = \ddot{y}(t_f) = y^{(3)}(t_i) = y^{(3)}(t_f) = 0$$

which yield $a_0 = 126$, $a_1 = -420$, $a_2 = 540$, $a_3 = -315$, and $a_4 = 70$.

The polynomial in (27) is often used as a reference trajectory in flatness-based control. A more general formulation can be found in [30].

IV. Output Feedback Control

The aforementioned state feedback controller requires the measurement of all the state variables, including the speed x_2. Usually, the gap between the electrodes and the charge on the device can be deduced from the input current, the voltage across the device, and the capacitance (see, e.g., [31]). However, direct sensing of velocity during normal operations for microdevices is extremely difficult. When the speed measurement is not available, we can use a certainty-equivalence implementation of state feedback design by replacing x_2 by its estimate obtained from an observer based on the measurement of deflection and charge. The observer design and the output feedback control synthesis are presented in the following.

A. Reduced-Order Speed Observer

It can be shown that system (2) [or equivalently (12)] with the deflection x (or x_1) and the charge q as outputs admits the observer canonical form, making it possible to find an observer with linear error dynamics [32]. This implies in particular that system (2) should be observable. To construct a reduced-order observer for the only unavailable state variable v (or x_2), we set

$$\xi = x_2 - k_v x_1 \tag{28}$$

where k_v is an arbitrary positive real number. Differentiating (28) yields

$$\dot{\xi} = -((2\zeta + k_v)k_v + 1)\, x_1 - (2\zeta + k_v)\xi + \frac{1}{3}x_3. \tag{29}$$

Let

$$\hat{x}_2 = \hat{\xi} + k_v x_1 \tag{30}$$

where $\hat{\xi}$ is given by

$$\dot{\hat{\xi}} = -((2\zeta + k_v)k_v + 1)\, x_1 - (2\zeta + k_v)\hat{\xi} + \frac{1}{3}x_3. \tag{31}$$

Denoting the estimation error by $\tilde{x}_2 = \hat{\xi} - \xi = \hat{x}_2 - x_2$, we obtain from (29) and (31) that

$$\dot{\tilde{x}}_2 = -(2\zeta + k_v)\tilde{x}_2 \tag{32}$$

which is globally exponentially stable at the origin with a decay rate determined by the observer gain k_v. This implies that (30) and (31) form an exponential observer.

As we have proved by construction that the estimation error dynamics are linearizable by output injection and are exponentially stable, system (2) is indeed observable.

B. Control Synthesis by Observer Backstepping

The output feedback control design is based on the technique of observer backstepping [20], which contains also three steps.

Step 1: Let us consider the control of subsystem (14a) with the estimated speed $\hat{x}_2$ as a virtual input. Let also $z_1 = x_1 - y_r$ be the position tracking error; then, the dynamics of z_1 are given by

$$\dot{z}_1 = x_2 - \dot{y}_r. \tag{33}$$

Select now a Lyapunov-like function

$$V_1 = \frac{1}{2}z_1^2 + \frac{1}{2}\tilde{x}_2^2.$$

The time derivative of V_1 along the solutions of (14a) is

$$\begin{aligned}\dot{V}_1 &= z_1(\hat{x}_2 - \dot{y}_r) - z_1\tilde{x}_2 - (2\zeta + k_v)\tilde{x}_2^2 \\ &= z_1(x_{2d} + z_2 - \dot{y}_r) - z_1\tilde{x}_2 - (2\zeta + k_v)\tilde{x}_2^2\end{aligned}$$

where $z_2 = \hat{x}_2 - x_{2d}$ and x_{2d} represents the desired input. If x_{2d} is chosen as

$$x_{2d} = \dot{y}_r - k_1 z_1 \tag{34}$$

then

$$\begin{aligned}\dot{V}_1 &= -k_1 z_1^2 - (2\zeta + k_v)\tilde{x}_2^2 - z_1\tilde{x}_2 + z_1 z_2 \\ &= -k_1 z_1^2 - (2\zeta + k_v)\left(\tilde{x}_2^2 + \frac{z_1\tilde{x}_2}{2\zeta + k_v}\right) + z_1 z_2.\end{aligned}$$

By completing the square, we obtain

$$\begin{aligned}\dot{V}_1 &= -k_1 z_1^2 - (2\zeta + k_v)\left(\tilde{x}_2^2 + \frac{z_1}{2(2\zeta + k_v)}\right)^2 \\ &\quad + \frac{z_1^2}{4(2\zeta + k_v)} + z_1 z_2 \\ &\le -\tilde{k}_1 z_1^2 + z_1 z_2\end{aligned} \tag{35}$$

where

$$\tilde{k}_1 = k_1 - \frac{1}{4(2\zeta + k_v)}. \tag{36}$$

Step 2: Consider now the subsystem (14a) and (14b) with x_3 as a virtual input and augment V_1 to yield

$$V_2 = V_1 + \frac{1}{2}z_2^2 + \frac{1}{2}\tilde{x}_2^2.$$

Since

$$\dot{x}_{2d} = \dot{\hat{x}}_{2d} + k_1\tilde{x}_2 \tag{37}$$

where

$$\dot{\hat{x}}_{2d} = \ddot{y}_r + k_1(\dot{y}_r - \hat{x}_2) \tag{38}$$

$$\dot{\tilde{x}}_2 = \dot{x}_2 + \dot{\hat{x}}_2 = -2\zeta x_2 - x_1 + \frac{1}{3}x_3 - (2\zeta + k_v)\tilde{x}_2 \tag{39}$$

the dynamics of z_2 can be written as

$$\dot{z}_2 = -2\zeta x_2 - x_1 + \frac{1}{3}x_3 - (2\zeta + k_v + k_1)\tilde{x}_2 - \dot{\hat{x}}_{2d}. \tag{40}$$

The time derivative of V_2 along the solutions of the corresponding subsystem is given by

$$\begin{aligned}\dot{V}_2 &= \dot{V}_1 + z_2\dot{z}_2 + \tilde{x}_2\dot{\tilde{x}}_2 \\ &\le -\tilde{k}_1 z_1^2 - (2\zeta + k_v)\tilde{x}_2^2 \\ &\quad + z_2\left(z_1 - 2\zeta\hat{x}_2 - x_1 + \frac{1}{3}x_3 - (k_v + k_1)\tilde{x}_2 - \dot{\hat{x}}_{2d}\right).\end{aligned}$$

Letting x_{3d} be the desired value for x_3 and noting that $z_3 = x_3 - x_{3d}$ and $\zeta = \zeta_0 + \Delta\zeta$, we have

$$\begin{aligned}\dot{V}_2 \le -\tilde{k}_1 z_1^2 - (2\zeta + k_v)\tilde{x}_2^2 + z_2\Big(z_1 - 2(\zeta + \Delta\zeta)\hat{x}_2 \\ - x_1 + \frac{1}{3}(z_3 - x_{3d}) - (k_v + k_1)\tilde{x}_2 - \dot{\hat{x}}_{2d}\Big)\Big).\end{aligned} \tag{41}$$

In order to counteract the uncertainty $\Delta\zeta$, a nonlinear damping term should be added to the stabilizing function. The desired input in this case is chosen to be the following:

$$x_{3d} = 3\left(-z_1 + x_1 + \dot{\hat{x}}_{2d} + 2\zeta_0\hat{x}_2 - k_2 z_2 - \kappa_2\zeta_0\hat{x}_2^2 z_2\right) \tag{42}$$

where κ_2 is the gain of the nonlinear damping term whose lower bound will be given later on.

It is shown in Appendix II that

$$\dot{V}_2 \le -\tilde{k}_1 z_1^2 - \tilde{k}_2 z_2^2 - (\kappa_2\zeta_0 - 1)\,\hat{x}_2^2 + \Delta\zeta^2 + \frac{1}{3}z_2 z_3 \tag{43}$$

where

$$\tilde{k}_2 = k_2 - \frac{(k_1 + k_v)^2}{4(2\zeta + k_v)^2}. \tag{44}$$

Step 3: By augmenting V_2, the Lyapunov function candidate for the closed-loop system is chosen to be

$$V_3 = \frac{1}{2}z_3^2 + \frac{1}{2}\tilde{x}_2^2 + V_2 = \frac{1}{2}z_1^2 + \frac{1}{2}z_2^2 + \frac{1}{2}z_3^2 + \frac{3}{2}\tilde{x}_2^2. \tag{45}$$

The time derivative of V_3 along the solutions of the closed-loop system satisfies

$$\begin{aligned}\dot{V}_3 \le &-\tilde{k}_1 z_1^2 - \tilde{k}_2 z_2^2 - (\kappa_2\zeta_0 - 1)\hat{x}_2^2 z_2^2 + \Delta\zeta^2 \\ &+ z_3\Bigg(\frac{1}{3}z_2 - 3(ab_1 + b_2) + 6\Delta\zeta b_1\hat{x}_2 - c\tilde{x}_2 \\ &\quad + \beta\Bigg(\frac{4\sqrt{x_3}}{3}u - 2x_3(1 - x_1) \\ &\qquad + 2r\rho_p\hat{x}_2 x_3 - 2r\rho_p\tilde{x}_2 x_3 - 2\rho_s x_3\Bigg)\Bigg)\end{aligned} \tag{46}$$

where

$$a = -x_1 - 2\zeta_0\hat{x}_2 + \frac{1}{3}x_3 \tag{47}$$

$$b_1 = 2\zeta_0 - k_1 - k_2 - 2\kappa_2\zeta_0\hat{x}_2 z_2 - \kappa_2\zeta_0\hat{x}_2^2 \tag{48}$$

$$b_2 = \dddot{y}_r + k_1\ddot{y}_r + \dot{y}_r + \left(k_2 + \kappa_2\zeta_0\hat{x}_2^2\right)\dot{\hat{x}}_{2d} \tag{49}$$

$$c = 3\left(k_1\left(k_2 + \kappa_2\zeta_0\hat{x}_2^2\right) - k_v b_1\right). \tag{50}$$

Let $U = (4/3)\sqrt{x_3}u$. The proposed backstepping controller is given by

$$\begin{aligned}U = &\,2x_3(1 - x_1) - \frac{1}{\underline{\beta}}k_3 z_3 - \frac{3}{\underline{\beta}}\left(ab_1 + b_2 - \frac{z_2}{9}\right) \\ &- \frac{1}{\underline{\beta}}\Big(\kappa_{31}\left(ab_1 + b_2 - \frac{z_2}{9}\right)^2 + \kappa_{32}\zeta_0\hat{x}_2^2 b_1^2 + \kappa_{33}\hat{x}_2^2 x_3^2 \\ &\quad + \kappa_{34}x_3^2 + \kappa_{35}\left(1 + x_3^2\right)c^2\Big)z_3\end{aligned} \tag{51}$$

with $k_3 > 0$, where κ_{31}, κ_{32}, κ_{33}, κ_{34}, and $\kappa_{35} > 0$ are the gains of the nonlinear damping terms. In conclusion, we have the following.

Theorem 2: For system (14) with the uncertainties satisfying Assumptions 1–3 and y_r being sufficiently smooth, the backstepping controller (51) with

$$\begin{aligned}&k_v - \frac{1 + 2\bar{\rho}_p^2}{8\kappa_{35}} > 0 \quad k_1 - \frac{1}{4k_v^2} \quad k_2 - \frac{(k_1 + k_v)^2}{4k_v^2} \\ &\kappa_2 > \frac{1}{\zeta_0} \quad \kappa_{31} > 1 \quad \kappa_{32} > \frac{1}{\zeta_0} \quad \kappa_{33} > 1 \quad \kappa_{34} > \frac{\bar{\rho}_s^2}{\underline{r}^2}\end{aligned} \tag{52}$$

renders the closed-loop error dynamics, including the speed observer, locally ISS with respect to the uniformly bounded inputs $\Delta\beta$, ρ_p, ρ_s, and $\Delta\zeta$. In light of this, the function V given by (45) is an ISS CLF. Furthermore, the ultimate bound for the tracking error z_1 can be rendered arbitrarily small by choosing the feedback gains k_1, k_2, and k_3 to be large enough.

Proof: See Appendix III. ■

Similar to the state feedback control, the actual control u is singular when $x_3 = 0$. In practice, we can use a control of the form (26) in order to avoid the singularity.

V. Simulation Study

In our simulation study, the nominal values of the parameters of the plant are $\zeta_0 = 1$, $r_0 = 1$, $\rho_p = 0$, and $\rho_s = 0$. The actuator is supposed to be driven by a bipolar voltage source. The boundaries of modeling errors and parametric uncertainties are $\bar{\rho}_s = 2$, $\bar{\rho}_p = 8$, $\underline{r} = 0.5$, and $\bar{r} = 2$ so that $\underline{\beta} = 0.0152$. Note that the upper bound of ρ_s is much higher than the one corresponding to the structures studied in Sections II-B and C. The upper bound $\bar{\rho}_p = 8$ should also represent a conservative estimation of parallel parasitics for microactuators with reasonable geometrical aspect ratio. Furthermore, the bounds on the value of the loop resistance r cover a wide range of variation (from 50% to 200% of the nominal value).

As the performance of the state feedback control is usually superior to its certainty-equivalence implementation, we

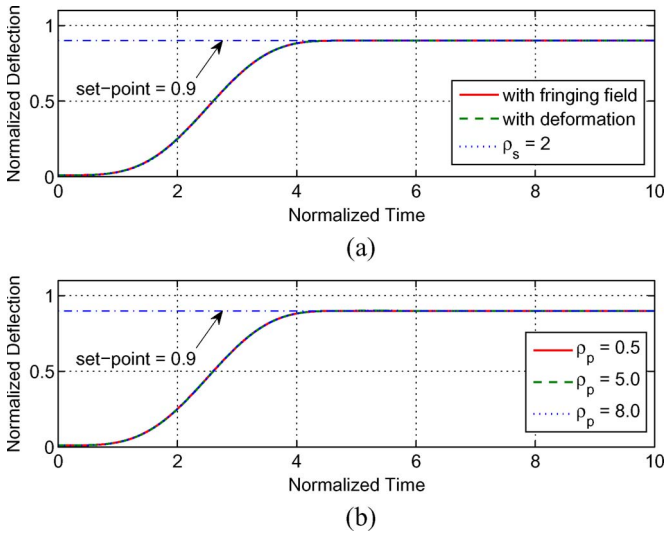

Fig. 8. Influence of serial and parallel capacitive uncertainties. (a) Variation of serial capacitive uncertainties. (b) Variation of parallel capacitive uncertainties.

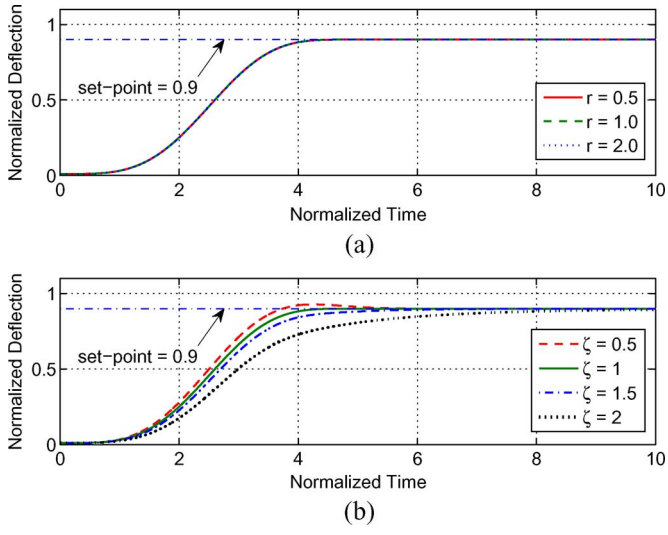

Fig. 9. Robustness against parametric uncertainties: (a) Variation of loop resistance. (b) Variation of damping ratio.

present only the simulation results for the output feedback control scheme. Note that, in the simulation, a small bias voltage is applied to the device in order to keep the moveable plate away from the origin, which is a singular point.

First, we consider only the influence of ρ_s and ρ_p. In the simulation, we tested different levels of serial and parallel capacitive uncertainties, while the damping ratio ζ and the loop resistance r are set to their nominal values. The set point is chosen to be 90% of a full gap deflection. Fig. 8(a) shows the simulation results of the devices presented in Sections II-B and C, which have a serial capacitance introduced by fringing fields and deformations, respectively. We also simulated a device with much higher level of serial capacitive uncertainty, where ρ_s is fixed to 2, corresponding to the worst case. Compared to the position prediction based on the simplified model (see Fig. 3 in Section II-A), the presented robust controller drastically improved the regulation accuracy. Fig. 8(b) shows the simulation results for different levels of parallel capacitive uncertainties. It can be seen that, in the range of variation of the parallel capacitive uncertainties, the system performs nearly identically.

The second test is concerned with the uncertainties in the damping ratio ζ and the loop resistance r. The device used in the simulation is the one presented in Section II-C, and the level of parallel capacitive uncertainties is fixed to $\rho_p = 1$. The set point is chosen to be 90% of a full gap deflection. It is shown in Fig. 9 that the system still performs very well even for very important parameter variations and that the performance is mostly influenced by the uncertainty related to the mechanical parameter, namely, the damping b.

In the last test, we considered 50% of a full gap deflection set-point control of the device presented in Section II-C. In the simulation, the parameter variations are set to $\Delta\zeta = -0.5$ and $\Delta r = 0.5$. Two different levels of parallel capacitive uncertainties are considered: $\rho_p = 1$ and $\rho_p = 5$. The state variables and control signals are shown in Fig. 10. It can be seen that the system responses are nearly identical for these two configurations; however, the control signals are significantly different. This shows the effect of the presented robust control scheme.

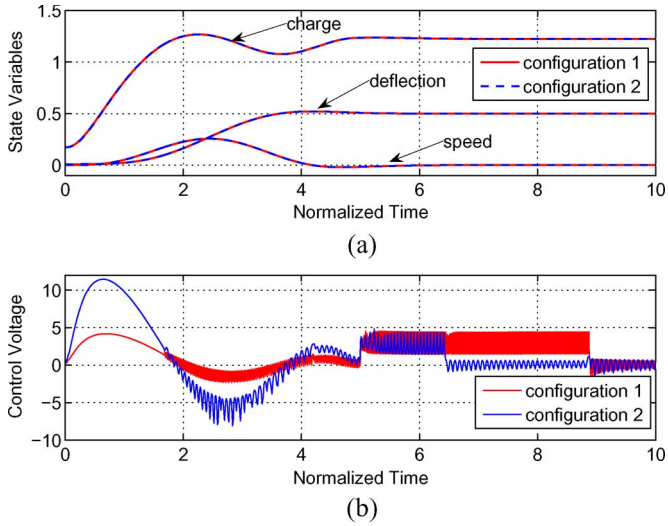

Fig. 10. Set-point control test. (a) State variables. (b) Control voltage.

Note that, due to the bias voltage applied, the charge is not zero at the initial point, which introduces a slight deflection.

Finally, it is worth noting that all the presented results have been obtained by using the same controller with the same tuning, which exhibits a satisfactory robustness.

VI. Conclusion

This paper investigated two of the most known modeling errors related to the simplified model of electrostatic parallel-plate microactuators: fringing field effect and deformations. The description of such phenomena requires the utilization of partial differential equations, resulting in complex mathematical models and difficulties in designing and implementing control systems. We have shown, by FEM-based simulations, that the modeling error due to fringing field effect and deformations can be compensated by a variable serial capacitor. Combined with an appropriate robust control scheme, an exact analytical

expression of the introduced serial capacitance is not required, but merely its boundary represented by capacitive influence coefficients. Based on a generic model of electrostatic parallel-plate microactuators, a state feedback robust control scheme using the technique of ISS, and backstepping design is derived. This algorithm has further been extended to the case where the speed measurement is not available. The stability of the closed-loop systems has been demonstrated through stability analysis, and the numerical simulations show that the proposed control systems exhibit satisfactory performance and robustness vis-à-vis capacitive and parametric uncertainties. Compared to adaptive backstepping control which can achieve asymptotic regulation by assuming a constant or slow-varying unknown parameter (see, e.g., [20]), the presented ISS controllers can handle arbitrary time-varying uncertainties. This feature is particularly suitable for dealing with state-dependent modeling errors. Note that the ISS framework can also deal with other types of uncertainties, such as sensor noise and disturbance rejection, allowing one to address the control of more generic and practical microdevices. Presenting different types of modeling errors by capacitive uncertainties, using numerical simulation or experimental measurements to determine the variation boundaries of these uncertainties, and then employing robust control techniques will considerably decrease modeling complexity while achieving enhanced performance and robustness.

APPENDIX I
DYNAMICS OF ELECTRICAL SUBSYSTEM WITH SERIAL AND PARALLEL CAPACITORS

Denoting by Q_p the charge on C_p and applying Kirchhoff laws yields

$$I_s R = V_s - V_p \tag{53}$$

$$I_s = I_a + I_p = \dot{Q}_a + \dot{Q}_p. \tag{54}$$

Since the voltage across the actuator is

$$V_a = \frac{C_s}{C_a + C_s} V_p = \frac{Q_a}{C_a} \tag{55}$$

it follows that

$$\frac{Q_p}{C_p} = V_p = \frac{C_a + C_s}{C_a C_s} Q \tag{56}$$

hence,

$$Q_p = \frac{C_p(C_a + C_s)}{C_a C_s} Q_a \tag{57}$$

$$\dot{Q}_p = -\frac{C_p Q}{C_a^2}\dot{C}_a + \frac{C_p(C_a + C_s)}{C_a C_s}\dot{Q}_a. \tag{58}$$

We can deduce from (53), (54), and (56) that

$$V_s - \frac{C_a + C_s}{C_a C_s} Q_a = R\left(\frac{C_a C_s + C_p(C_a + C_s)}{C_a C_s}\dot{Q}_a - \frac{C_p Q_a}{C_a^2}\dot{C}_a\right)$$

or, equivalently

$$\dot{Q}_a = \frac{C_a C_s}{R(C_a C_s + C_a C_p + C_s C_p)} \times \left(V_s - \left(\frac{C_a + C_s}{C_a C_s} - \frac{R C_p}{C_a^2}\dot{C}_a\right) Q_a\right) \tag{59}$$

which can then be rewritten as (5).

APPENDIX II
UPPER BOUND OF $\dot{V}_2$ IN (43)

For x_{3d} given by (42), we have

$$\begin{aligned}\dot{V}_2 \leq & -\tilde{k}_1 z_1^2 - (2\zeta + k_v)\tilde{x}_2^2 - k_2 z_2^2 \\ & - \kappa_2 \zeta_0 \hat{x}_2^2 z_2^2 - z_2\left(2\Delta\zeta\hat{x}_2^2 + (k_v + k_1)\tilde{x}_2\right) + \frac{1}{3} z_2 z_3 \\ \leq & -\tilde{k}_1 z_1^2 - (2\zeta + k_v)\tilde{x}_2^2 - \kappa_2 \zeta_0 \hat{x}_2^2 z_2^2 \\ & - (k_v + k_1)\tilde{x}_2 z_2 + 2|\Delta\zeta||\hat{x}_2 z_2| + \frac{1}{3} z_2 z_3.\end{aligned} \tag{60}$$

By completing the square, we obtain

$$\dot{V}_2 \leq -\tilde{k}_1 z_1^2 - \tilde{k}_2 z_2^2 - \kappa_2 \zeta_0 \hat{x}_2^2 z_2^2 + 2|\Delta\zeta||\hat{x}_2 z_2| + \frac{1}{3} z_3. \tag{61}$$

Applying Young's inequality, we can then deduce (43) from (61).

APPENDIX III
PROOF OF THEOREM 2

Substituting the input in (46) by the backstepping controller (51) and taking into account bounds (15), (17), (18), and (43) yields

$$\begin{aligned}\dot{V}_3 = & -\tilde{k}_1 z_1^2 - \tilde{k}_2 z_2^2 - \frac{\beta}{\underline{\beta}} k_3 z_3^2 - (\kappa_2 \zeta_0 - 1)\hat{x}_2^2 z_2^2 + \Delta\zeta^2 \\ & - (2\zeta + k_v)\tilde{x}_2^2 + \left(6 b_1 \Delta\zeta \hat{x}_2 z_3 - \frac{1}{\underline{\beta}} \kappa_{32} \zeta_0 b_1^2 \hat{x}_2^2 z_3^2\right) \\ & + \left(\left(\frac{1}{3} z_2 - 3(a b_1 + b_2) + \frac{3\beta}{\underline{\beta}}\left(a b_1 + b_2 - \frac{z_2}{9}\right)\right) z_3 \right. \\ & \left. - \frac{\beta}{\underline{\beta}} \kappa_{31}\left(a b_1 + b_2 - \frac{z_2}{9}\right)^2 z_3^2\right) \\ & + \left(2 r \rho_p \beta \hat{x}_2 x_3 z_3 - \frac{\beta}{\underline{\beta}} \kappa_{33} \hat{x}_2^2 x_3^2 z_3^2\right) \\ & - \left(2\rho_s \beta x_3 z_3 + \frac{\beta}{\underline{\beta}} \kappa_{34} x_3^2 z_3^2\right) + \left(d\tilde{x}_2 z_3 - \frac{\beta}{\underline{\beta}} \kappa_{35} d^2 z_3^2\right) \\ & - \left(2 r \rho_p \beta d \tilde{x}_2 x_3 z_3 + \frac{\beta}{\underline{\beta}} \kappa_{35} d^2 x_3^2 z_3^2\right).\end{aligned} \tag{62}$$

Applying Young's inequality and noting that $\beta \geq \underline{\beta}$ and

$$\beta r \leq 1/\left(1 + \rho_p(2 + \rho_s)\right)$$

$\dot{V}_3$ can be further bounded as follows:

$$\begin{aligned}\dot{V}_3 \leq & -\tilde{k}_1 z_1^2 - \tilde{k}_2 z_2^2 - k_3 z_3^2 - (\kappa_2\zeta_0 - 1)\hat{x}_2^2 z_2^2 \\ & - \left(\frac{\beta}{\underline{\beta}}\kappa_{31} - 1\right)\left(ab_1 + b_2 - \frac{z_2}{9}\right)^2 z_3^2 \\ & - \left(\frac{\beta}{\underline{\beta}}\kappa_{32}\zeta_0 - 1\right) b_1^2 \hat{x}_2^2 z_3^2 - \left(\frac{\beta}{\underline{\beta}}\kappa_{33} - 1\right)\hat{x}_2^2 x_3^2 z_3^2 \\ & - \left(\frac{\beta}{\underline{\beta}}\kappa_{34} - \frac{\overline{\rho}_s^2}{\underline{r}^2}\right) x_3^2 z_3^2 - \left((2\zeta + k_v) - \frac{1 + 2\overline{\rho}_p^2}{8\kappa_{35}}\right) \\ & + 10\Delta\zeta^2 + \frac{9}{4}\Delta\beta^2 + \frac{\rho_p^2 + \rho_s^2}{\left(1 + \rho_p(2 + \rho_s)\right)^2}. \end{aligned} \tag{63}$$

If (52) is satisfied, then

$$\dot{V}_3 \leq -\alpha(z) + 10\Delta\zeta^2 + \frac{9}{4}\Delta\beta^2 + \frac{\rho_p^2 + \rho_s^2}{\left(1 + \rho_p(2 + \rho_s)\right)^2} \tag{64}$$

where

$$\alpha(z) = -\tilde{k}_1 z_1^2 - \tilde{k}_2 z_2^2 - k_3 z_3^2$$

is obviously of class $\mathcal{K}_\infty$. Noting that $(\rho_p^2 + \rho_s^2)/(1 + \rho_p(2 + \rho_s))^2$ is uniformly bounded, we conclude that the closed-loop error dynamics are ISS with $\Delta\zeta$, ρ_p, ρ_s, and $\Delta\beta$ as the inputs.

ACKNOWLEDGMENT

The authors would like to thank the anonymous reviewers for their insightful and constructive comments which have greatly improved the presentation of our work.

REFERENCES

[1] S. D. Senturia, *Microsystem Design*. Norwell, MA: Kluwer, 2002.
[2] N. Doble and D. R. Williams, "The application of MEMS technology for adaptive optics in vision science," *IEEE J. Sel. Topics Quantum Electron.*, vol. 10, no. 3, pp. 629–635, May/Jun. 2004.
[3] B. Palmer, "Capacitance of a parallel-plate capacitor by the Schwarz-Christoffel transformation," *Trans. AIEE*, vol. 56, no. 3, pp. 363–366, Mar. 1937.
[4] R. S. Elliott, *Electromagnetics*. New York: McGraw-Hill, 1966.
[5] W. H. Chang, "Analytical IC metal-line capacitance formulas," *IEEE Trans. Microw. Theory Tech.*, vol. MTT-24, no. 9, pp. 608–611, Sep. 1976.
[6] C. P. Yuan and T. N. Trick, "A simple formula for the estimation of the capacitance of two-dimensional interconnects in VLSI circuits," *IEEE Electron Device Lett.*, vol. EDL-3, no. 12, pp. 391–393, Dec. 1982.
[7] T. Sakurai and K. Tamaru, "Simple formulas for two- and three-dimensional capacitances," *IEEE Trans. Electron Devices*, vol. ED-30, no. 2, pp. 183–185, Feb. 1983.
[8] N. V. de Meijs and J. T. Fokkema, "VLSI circuit reconstruction from mask topology," *Integration*, vol. 2, no. 2, pp. 85–119, 1984.
[9] G. J. Sloggett, N. G. Barton, and S. J. Spencer, "Fringing fields in disc capacitors," *J. Phys. A, Math. Gen.*, vol. 19, no. 14, pp. 2725–2736, Oct. 1986.
[10] A. H. Nayfeh and P. F. Pai, *Linear and Nonlinear Structural Mechanics*. New York: Wiley, 2004.
[11] V. Varadan, K. Vinoy, and S. Gopalakrishnan, *Smart Material Systems and MEMS: Design and Development Methodologies*. Hoboken, NJ: Wiley, 2006.
[12] E. T. Ong and K. M. Lim, "Three-dimensional singular boundary elements for corner and edge singularities in potential problems," *Eng. Anal. Bound. Elem.*, vol. 29, no. 2, pp. 175–189, Feb. 2005.
[13] J. A. Pelesko and D. H. Bernstein, *Modeling MEMS and NEMS*. Boca Raton, FL: CRC Press, 2003.
[14] A. F. Marqus, R. C. Castell, and A. Shkel, "Modelling the electrostatic actuation of MEMS: State of the art 2005," Universitat Politecnica de Catalunya, Barcelona, Spain, Tech. Rep. IOC-DT-P-2005-18, 2005. [Online]. Available: http://hdl.handle.net/2117/119
[15] A. Bensoussan, G. D. Prato, M. C. Delfour, and S. K. Mitter, "Representation and control of infinite dimensional systems," in *Systems & Control: Foundations & Applications*, 2nd ed. New York: Birkhäuser, 2007.
[16] E. K. Chan and R. W. Dutton, "Electrostatic micromechanical actuator with extended range of travel," *J. Microelectromech. Syst.*, vol. 9, no. 3, pp. 321–328, Sep. 2000.
[17] M. Hosseini, G. Zhu, and Y.-A. Peter, "A new formulation of fringing capacitance and its application to the control of parallel-plate electrostatic micro actuators," *Analog Integr. Circuits Signal Process.*, vol. 55, no. 2/3, pp. 119–128, Dec. 2007.
[18] E. D. Sontag, "Smooth stabilization implies coprime factorization," *IEEE Trans. Autom. Control*, vol. 34, no. 4, pp. 435–443, Apr. 1989.
[19] E. D. Sontag, "The ISS philosophy as a unifying framework for stability-like behavior," in *Nonlinear Control in the Year 2000*, vol. 2, A. Isidori, F. Lamnabhi- Lagarrigue, and W. Respondek, Eds. Berlin, Germany: Springer-Verlag, 2000, pp. 443–468.
[20] M. Krstić, I. Kanellakopoulos, and P. Kokotoviæ, *Nonlinear and Adaptative Control Design*. New York: Wiley, 1995.
[21] G. Zhu, J. Penet, and L. Saydy, "Modeling and control of electrostatically actuated MEMS in the presence of parasitics and parametric uncertainties," *Trans. ASME, J. Dyn. Syst. Meas. Control*, vol. 129, no. 6, pp. 786–794, Nov. 2007.
[22] J. Pont-Nin, A. Rodríguez, and L. Castañer, "Voltage and pull-in time in current drive of electrostatic actuators," *J. Microelectromech. Syst.*, vol. 11, no. 3, pp. 196–205, Jun. 2002.
[23] G. Zhu, J. Lévine, and L. Praly, "On the differential flatness and control of electrostatically actuated MEMS," in *Proc. Amer. Control Conf.*, Portland, OR, Jun. 8–10, 2005, pp. 2493–2498.
[24] D. H. S. Maithripala, J. M. Berg, and W. P. Dayawansa, "Control of an electrostatic MEMS using static and dynamic output feedback," *Trans. ASME, J. Dyn. Syst. Meas. Control*, vol. 127, no. 3, pp. 443–450, Sep. 2005.
[25] M. Andrews, I. Harris, and G. Turner, "A comparison of squeeze-film theory with measurements on a microstructure," *Sens. Actuators A, Phys.*, vol. 36, no. 1, pp. 79–87, Mar. 1993.
[26] D. H. S. Maithripala, J. M. Berg, and W. P. Dayawansa, "Nonlinear dynamic output feedback stabilization of electrostatically actuated MEMS," in *Proc. 42nd IEEE Conf. Decision Control*, Maui, HI, Dec. 2003, pp. 61–66.
[27] Z. P. Jiang, A. Teel, and L. Praly, "Small-gain theorem for ISS systems and applications," *Math. Control Signals Syst.*, vol. 7, no. 2, pp. 95–120, Jun. 1994.
[28] Z. P. Jiang, I. Mareels, and J.-B. Pomet, "Output feedback global stabilization for a class of nonlinear systems with unmodeled dynamics," *Eur. J. Control*, vol. 2, no. 6, pp. 201–210, 1996.
[29] Z. P. Jiang and I. Mareels, "A small gain control method for nonlinear cascaded systems with dynamic uncertainties," *IEEE Trans. Autom. Control*, vol. 42, no. 3, pp. 292–308, Mar. 1997.
[30] J. Lévine, *Analyse et Commande des Systmes Non Linaires*, 2004. [Online]. Available: http://cas.ensmp.fr/%7Elevine/Enseignement/CoursENPC.pdf
[31] R. C. Anderson, B. Kawade, D. H. S. Maithripala, K. Ragulan, J. M. Berg, and R. O. Gale, "Integrated charge sensors for feedback control of electrostatic MEMS," in *Proc. SPIE Conf. Smart Struct. Mater.*, San Diego, CA, Mar. 2005, pp. 42–53.
[32] A. Isidori, *Nonlinear Control Systems*, 3rd ed. London, U.K.: Springer-Verlag, 1995.

Guchuan Zhu (M'07) received the M.S. degree in electrical engineering from Beijing Institute of Aeronautics and Astronautics, Beijing, China, in 1982, the Ph.D. degree in mathematics and control from the École des Mines de Paris, Paris, France, in 1992, and the Graduate Diploma in computer science from Concordia University, Montréal, QC, Canada, in 1999.

Prior to joining the École Polytechnique de Montréal, Montréal, in 2004, where he is currently an Assistant Professor in the Electrical Engineering Department, he was a Lecturer with the Department of Electronic Engineering, Beijing Institute of Aeronautics and Astronautics, a Postdoctoral Researcher and Research Fellow with the École de Technologie Supérieure, Montréal, and a Software Designer with SR Telecom Inc., Montréal. His current research interests include nonlinear system control with applications to microsystems.

Lahcen Saydy was born in Tafraout, Morocco. He received the "Ingénieur d'état" degree from EMI Engineering School, Rabat, Morocco, in 1979, and the M.Sc. and Ph.D. degrees in electrical engineering from the University of Maryland, College Park, in 1985 and 1988, respectively.

From 1979 to 1981, he was a "Maître Assistant" with the Physics Department, University Caddi Ayyad, Marrakech, Morocco. He spent 1989 with the Institute for Systems Research, University of Maryland, as a Postdoctoral Fellow and joined the Electrical Engineering Department, École Polytechnique de Montréal, Montréal, QC, Canada, where he is currently an Associate Professor. His research interests are in control system design, particularly robust stability and control, with application to the areas of flight control and electric power systems.

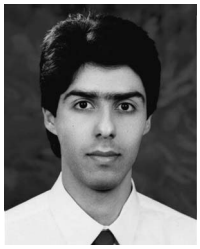

Mehran Hosseini received the B.Sc. degree in electrical engineering from Isfahan University of Technology, Isfahan, Iran, in 1993, and the M.A.Sc. degree in electrical engineering from Concordia University, Montreal, QC, Canada, in 2005. He is currently working toward the Ph.D. degree in the Engineering Physics Department, École Polytechnique Montreal, Montréal.

He investigates microelectromechanical systems, and his research focuses on modeling, simulation, and fabrication of electrostatically actuated micromirrors.

Jean-François Chianetta received the M.S. degree in mechanical engineering from the Faculté Polytechnique de Mons, Mons, Belgium, in 2006.

In 2006, he did a final study project related to micromirror control with the Micro and Nano Systems Laboratory, Engineering Physics Department, École Polytechnique de Montréal, Montréal, QC, Canada. He is currently with Coventor, Paris, France, as a Software Development Engineer, where he is developing tools for microsystems design.

Yves-Alain Peter (S'93–A'03–M'03–SM'07) received the M.S. and Ph.D. degrees in physics from the University of Neuchâtel, Neuchâtel, Switzerland, in 1994 and 2001, respectively.

Currently, he is an Associate Professor and Scientific Director of the Laboratory for Microfabrication, Engineering Physics Department, École Polytechnique de Montréal, Montréal, QC, Canada. In 1995, he was a Research Associate with the Medical Radiobiology Department, Paul Scherrer Institute, Switzerland. During 1995–2001, he was a Graduate Research Assistant with the Applied Optics Group, Institute of Microtechnology, University of Neuchâtel. From 2001 to 2003, he was a Postdoctoral Researcher with the Microphotonics Group, Stanford University, Stanford, CA. He was an R&D Engineer and Project Leader with the Swiss Center for Electronics and Microtechnology, Switzerland, from 2003 to 2004. His research interests include micro and nano optoelectromechanical systems with applications in adaptive optics and tunable nanophotonics structures.

Dr. Peter is a member of the IEEE Lasers and Electro-Optics Society, the Optical Society of America, and the Swiss Physical Society.